

Particle Dispersion under Tidal Bores: Application to Sediments and Fish Eggs

Hubert Chanson and Kok-Keng Tan

The University of Queensland, School of Civil Engineering
Brisbane QLD 4072, Australia
E-mail: h.chanson@uq.edu.au

Keywords: tidal bores, turbulent mixing, particle dispersion

Abstract

A tidal bore is a surge of water propagating upstream as the tidal flow turns to rising into an estuary with a tidal range larger than 5 to 6 m and a bathymetry that amplifies the tidal wave. The bore front is a shock characterised by a singularity of the free-surface and pressure and velocity fields. This study aims to characterise the tidal bore propagation and the induced turbulent mixing under controlled flow conditions. Some physical modelling was performed based upon a Froude similitude and the tracking of light particles was conducted with both undular and breaking bores. Some large fluctuations of horizontal and vertical particle velocity components were observed during the undular bore propagation beneath the undulations. A major result was the identification of large-scale vortical structures generated below the front of the tidal bore. These large coherent turbulent structures must be responsible for some bed erosion and vertical mixing of the water column when a tidal bore propagates upstream in the estuarine zone of a natural system. The large-scale eddies are also responsible to the rapid longitudinal dispersion of fish eggs reducing the impact of predators, with some form of preferential motion depending upon the eggs' vertical elevation.

Introduction

A tidal bore forms during spring tide conditions when the tidal range exceeds 5 to 6 m and the flood tide is confined to a narrow funnelled estuary (Chanson 2010a). A bore is a surge of water propagating upstream as the tidal flow turns to rising. When the ocean level at the river mouth rises with time during the early flood tide, the leading edge of the tidal wave becomes steeper and steeper, until it forms an abrupt front that is the tidal bore (Fig. 1). The bore is a fascinating, intense and powerful natural phenomenon, attracting tourists, kayakers and surfers (Fig. 1a). However, the tidal bore processes remain poorly understood today because of a lack of field observations and comprehensive studies (Simpson et al. 2004, Wolanski et al. 2004).

A tidal bore is a positive surge associated with a discontinuity in water depth and a sudden rise of the water elevation. The bore front is a shock characterised by a singularity of the water depth and pressure and velocity fields. In Nature, a tidal bore may have a variety of different shapes (Fig. 1). The photographs illustrate in particular that the bore front is not a sharp, vertical discontinuity of the water surface because of the necessary curvature of the streamline and the associated pressure and velocity redistributions.

In absence of detailed field measurements, it is the aim of this study to characterise the tidal bore propagation and the induced turbulent mixing under controlled flow conditions. This was achieved through some physical modelling based upon a Froude dynamic similarity. The tracking of light particles was conducted with both undular and breaking

bores to provide some new Lagrangian description of the particle mixing processes beneath the tidal bore front. The results complement earlier Eulerian velocity measurements performed in the same facility, and provide a new understanding of the turbulent mixing and dispersion of particulates such as light sediment materials and fish eggs.



(a) Undular tidal bore of the Dordogne River on 30 Sept 2008 afternoon - The kayakers rode the 2nd wave crest while the surfer was ahead of the 3rd wave crest



(b) Sélune river tidal bore on 19 Sept. 2008 morning - Bore propagating from left to right - Note the breaking front in the foreground and the undulations in the deeper section

Figure 1: Photographs of tidal bores.

Nomenclature

a_w	wave amplitude (m)
B	channel width (m)
D_x	turbulent mixing coefficient (m^2s^{-1}) in the x-direction
D_z	turbulent mixing coefficient (m^2s^{-1}) in the z-direction
d_o	initially steady flow depth (m)
Fr	tidal bore Froude number
f	Darcy-Weisbach friction factor
g	gravitational acceleration (ms^{-2})
L_w	wave length (m)
Q	initially steady flow rate (m^3s^{-1})
q	discharge per unit width (m^2s^{-1}): $q = Q/B$
s	particle specific density
U	tidal bore celerity (ms^{-1}) for an observer standing on the bank, positive upstream
t	time (s)
t'	time (s) with $t'=0$ when the particle passed beneath the bore front
V_o	initially steady flow velocity (ms^{-1})
w_s	particle fall velocity (ms^{-1}) in still water
X	longitudinal co-ordinate (m)
x	longitudinal co-ordinate (m) measured from the test section upstream end, positive downstream
x'	longitudinal co-ordinate (m) positive downstream with $x'=0$ when the particle passed beneath the bore front
z	vertical elevation (m) positive upwards
Greek symbols	
ε_z	vertical mixing coefficient (m^2s^{-1}) in fully-developed open channel flows
σ_x	mean square displacement (m) of particles in the x-direction
σ_z	mean square displacement (m) of particles in the z-direction
\varnothing	diameter (m)
Subscripts	
avg	ensemble-average
o	initially steady flow conditions

x	longitudinal component
z	vertical component

Experimental Facility

The experiments were performed in a 12 m long 0.5 m wide rectangular open channel test section (Fig. 2). The flume was horizontal and made of smooth PVC bed and glass walls. The waters were supplied by a constant head tank feeding a large intake basin (2.1 m long, 1.1 m wide, 1.1 m deep) leading to the test section through a bed and sidewall convergent. A radial gate was located at the channel downstream end ($x = 11.9$ m) where x is the longitudinal distance from the channel test section upstream end and was used to control the initial water depth; its position did not change during an experiment. A fast-closing tainter gate was also located at $x = 11.15$ m and the gate was closed rapidly (completely or partially) to generate the tidal bore propagating upstream in the channel.

The initially steady discharge was measured with two orifice meters that were designed based upon the British Standards (1943). In steady flows, the water depths were measured using rail mounted pointer gauges. The bore propagation was studied with a series of acoustic displacement meters Microsonic™ Mic+25/IU/TC located along the channel between $x = 10.8$ and 4 m, and above the water surface (Fig. 3). Further observations were recorded between $x = 5.65$ and 4.85 m using a digital video camera Panasonic NV-GS300 (30 fps) and digital still cameras.

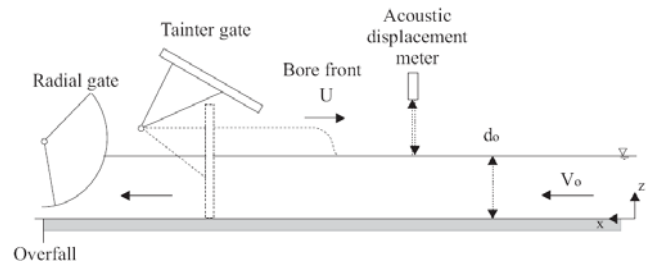


Figure 2: Sketch of the channel test section.

Generation of the tidal bore

The experimental geometry and configuration were chosen to have an initially steady open channel flow with a discharge Q between 0.013 and 0.058 m^3s^{-1} (Table 1). The opening of the downstream radial gate controlled the initial steady flow depth d_o and velocity V_o .

The tidal bore was generated by the rapid closure of the downstream tainter gate. The gate was identical to that used by Koch and Chanson (2008,2009) and Chanson (2010b); its closure time was less than 0.2 s. After the rapid closure, the bore propagated upstream (Fig. 3) and each run was stopped when the tidal bore front reached the upstream intake structure ($x < 0$), to avoid any wave reflection in the test section.

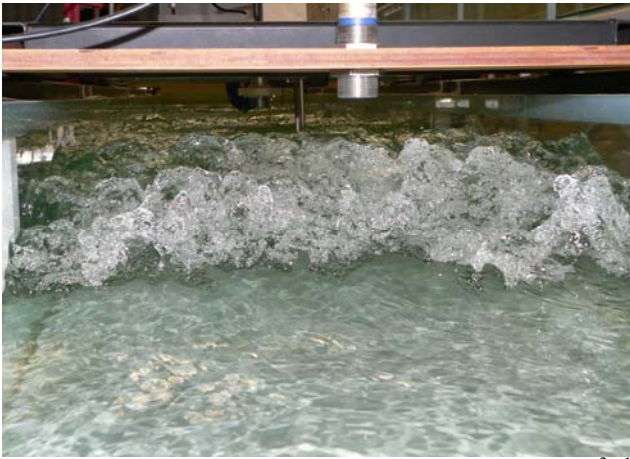


Figure 3: Breaking tidal bore ($Fr = 1.5$, $Q = 0.0578 \text{ m}^3\text{s}^{-1}$, $d_o = 0.139 \text{ m}$) - Looking at the incoming bore - Note the displacement meter sensor above the bore front and the pointer gauge in background.

Ref.	Q m^3s^{-1}	d_o m	U ms^{-1}	Fr	Comment
Hornung et al. (1995)	0	--	--	1.5 to 6	Smooth bed.
Koch & Chanson (2009)	0.040	0.079	0.14 to 0.68	1.3 to 2.0	$B = 0.5 \text{ m}$. Smooth bed.
Chanson (2010b)	0.058	0.14	0.5 to 0.9	1.1 to 1.5	$B = 0.5 \text{ m}$. Smooth & rough beds.
Present study	0.013 to 0.058	0.0505 to 0.196	0.33 to 1.19	1.01 to 1.7	$B = 0.5 \text{ m}$. Smooth bed.

Table 1: Experimental investigations of tidal bores.

Q m^3s^{-1}	V_o ms^{-1}	d_o m	U ms^{-1}	Fr	Type of tidal bore
0.013	0.335	0.0775	0.67	1.15	Undular bore.
	0.515	0.0505	0.55	1.51	Breaking bore.

Table 2: Particle tracking experiments in undular and breaking tidal bores (Present study).

Particles and particle tracking experiments

For one initial discharge, the turbulent mixing of light-weight particles was systematically recorded between $x = 5.65$ and 4.85 m with an undular bore and a breaking bore (Table 2). The particles were spherical-shaped beads with an average diameter of $3.72 \text{ mm} \pm 0.2 \text{ mm}$. Their relative density was deduced from some particle fall velocity experiments conducted in a 2 m high, 0.10 m \varnothing water column. The experimental data yielded a particle fall velocity $w_s = 0.047 \pm 0.012 \text{ m/s}$ corresponding to a relative density $s = 1.037 \pm 0.012$.

The particle density corresponded to some light-weight particles slightly heavier than water. Their diameter and density were close to those of striped bass (*Morone saxatilis*) fish eggs. In the Bay of Fundy, Rulifson and Tull (1999) observed typical fish egg diameters of about 4 mm with a specific density s between 1.0016 and 1.0066 depending upon their stages of development. The lightest eggs were unfertilised water hardened eggs. Fertilised eggs less than 10 hours old had a relative density of 1.0029 and

the heaviest eggs were in the final stages of development (Rulifson and Tull 1999).

In the present study, the particles were injected on the channel centreline and advected downstream by the initially steady flow. Their turbulent mixing in the bore front was recorded through the glass sidewalls using the video camera Panasonic NV-GS300.

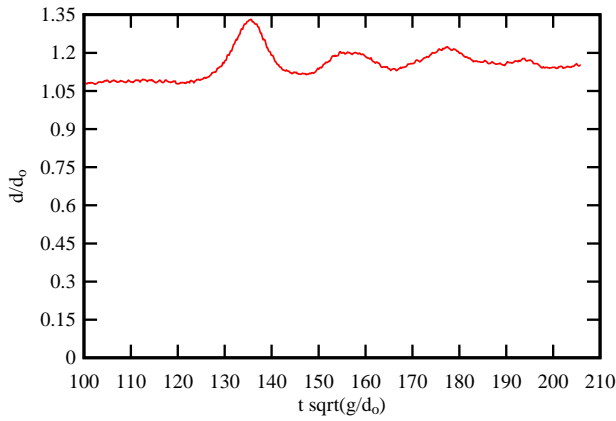
Basic Flow Patterns

Some visual observations and free-surface measurements were conducted for a range of flow conditions with initially-steady subcritical open channel flow (Table 1). Several flow patterns were observed depending upon the tidal bore Froude number $Fr = (V_o + U) / \sqrt{g d_o}$ where d_o is the initial flow depth, V_o is the initial flow velocity positive downstream, g is the gravity acceleration and U is the surge front celerity for an observer standing on the bank and positive upstream. Fr is the Froude number defined in the system of co-ordinates in translation with the tidal bore. For a Froude number between unity and 1.5 to 1.6 , the tidal bore was undular: that is, the wave front was followed by a train of secondary, quasi-periodic waves called undulations (Fig. 1a). For larger Froude numbers, a breaking bore was observed (Fig. 1b & 3). The basic flow pattern observations were consistent with the earlier findings of Favre (1935), Benet and Cunge (1971) and Treske (1994). Two examples of undular and breaking bore profiles are shown in Figure 4, presenting in dimensionless form the water depth as a function of time.

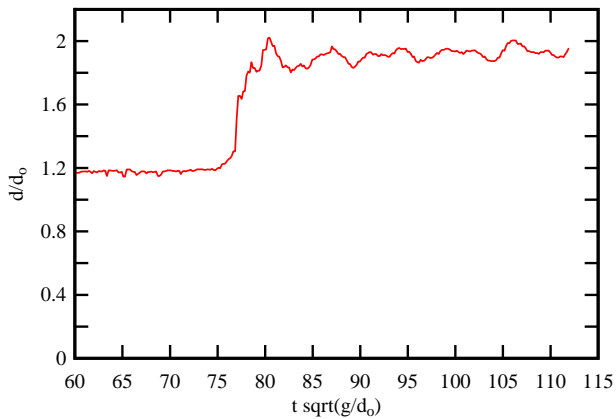
The undular tidal bore had a smooth, quasi-two-dimensional free-surface profile for $Fr < 1.2$ to 1.25 . For 1.2 to $1.25 < Fr$, some slight cross-waves (shock waves) were observed, starting next to the sidewalls upstream of the first wave crest and intersecting next to the first crest on the channel centreline. For $1.35 < Fr < 1.5$ to 1.6 , some slight wave breaking was observed at the bore front, and the secondary waves were flatter. The findings were comparable to those of earlier studies (Koch and Chanson 2009, Chanson 2010b).

At the largest bore Froude numbers (i.e. $Fr > 1.5$ to 1.6), the bore had a marked roller, and appeared to be quasi-two-dimensional (Fig. 3). Behind the roller, the free-surface was about horizontal although large free-surface fluctuations were observed. Some air entrainment and intense turbulent mixing was observed in the bore roller.

Note that the flow patterns were basically independent of the initially steady flow Froude number $V_o / \sqrt{g d_o}$, while an earlier study showed that these were also independent of the bed roughness (Chanson 2010b).



(a) Undular tidal bore ($Fr = 1.20$, $Q = 0.025 \text{ m}^3\text{s}^{-1}$, $d_0 = 0.107 \text{ m}$, $U = 0.73 \text{ ms}^{-1}$)



(b) Breaking tidal bore ($Fr = 1.56$, $Q = 0.058 \text{ m}^3\text{s}^{-1}$, $d_0 = 0.1315 \text{ m}$, $U = 0.99 \text{ ms}^{-1}$)

Figure 4: Instantaneous dimensionless free-surface profiles (measurements at $x = 5 \text{ m}$).

Free-surface undulation properties

A key feature of the undular tidal bores is the pseudo-periodic appearance of the secondary waves. The characteristics of the undulations were systematically recorded for three discharges ($Q = 0.025, 0.040 \text{ \& } 0.058 \text{ m}^3\text{s}^{-1}$) and for a range of initial flow depths for each flow rate (Table 1). Some typical results are shown in Figures 5 and 6 in terms of the dimensionless wave length L_w/d_0 and steepness a_w/L_w , where a_w and L_w are respectively the wave amplitude and steepness of the first length. The present experimental data are compared with the linear wave theory and Boussinesq equation solution in Figures 5 and 6. While the wave length decayed exponentially with increasing Froude number, the wave steepness data exhibited a local maximum about $Fr = 1.3$ to 1.4 . It is believed that the apparition of some wave breaking for $Fr > 1.35$ was responsible for the lesser energy dissipated in the secondary wave motion at larger Froude numbers and hence the smaller wave steepness for $Fr > 1.3$ to 1.4 .

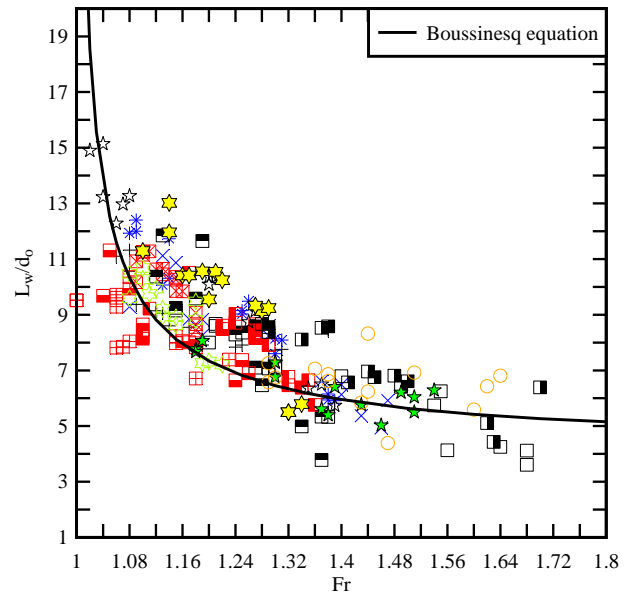


Figure 5: Dimensionless wave length of the first wave length of undular tidal bores - Comparison between present data and the Boussinesq equation (Andersen 1978).

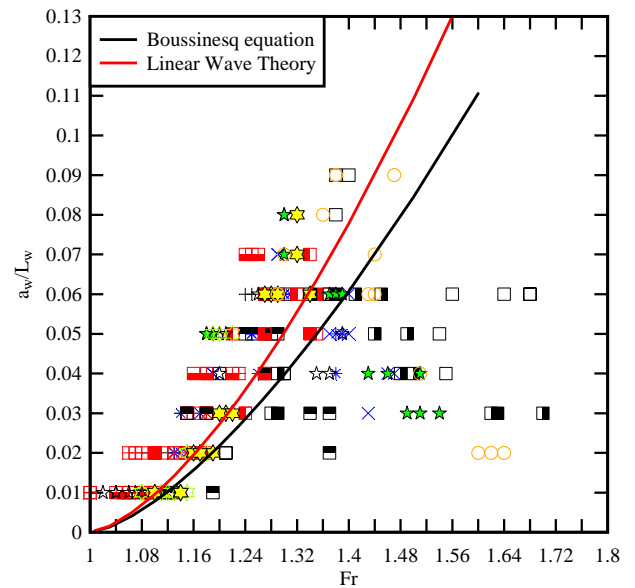


Figure 6: Dimensionless wave steepness of the first wave length of undular tidal bores - Comparison between present data, the Boussinesq equation (Andersen 1978) and the linear wave theory (Lemoine 1948).

Particle Tracking Results

For a constant initial discharge, the particle dispersion in undular and breaking tidal bores were tested (Table 2). Figure 7 presents some instantaneous free-surface profiles for both experiments. The observations were recorded at about $x = 5 \text{ m}$ where the bore propagated upstream with a constant celerity U . The distinctive shape of the first wave length is illustrated; for the undular bore experiment, the wave period was about 0.8 s . In Figure 7, the data are presented as the dimensionless water depth d/d_0 as a function of the longitudinal distance X/d_0 , where d is the

water depth measured above the bed and X is a longitudinal co-ordinate positive in the downstream direction. (The origin of X was $x = 4.85$ m in Figure 7.)

Some typical particle trajectories are presented in Figures 8 and 9 for the undular and breaking tidal bores respectively. Figures 8 and 9 show some sideview of the particle trajectories. In each graph, the horizontal axis is the longitudinal coordinate x' positive downstream with $x' = 0$ when the particle passed beneath the leading edge of the bore front and the vertical axis is the particle vertical elevation z . Each trajectory starts at $x' = 0$ and the time interval between each data point is $1/30$ s. On the graphs, the tidal bore propagates from left to right with x' positive to the left as in Figure 2.

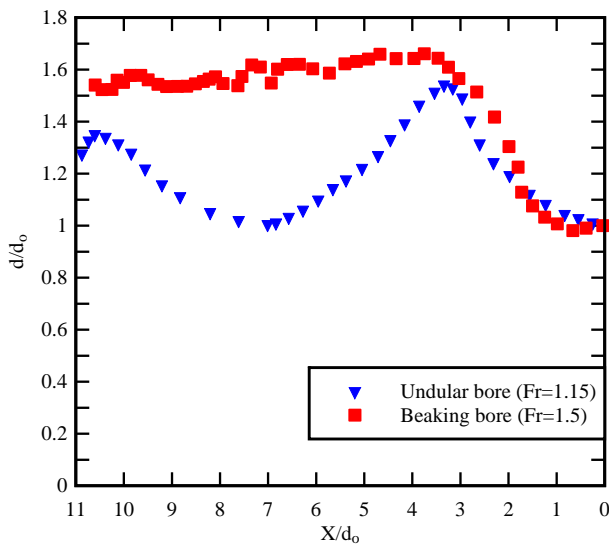


Figure 7: Dimensionless instantaneous free-surface profiles of tidal bores for the particle tracking experiments ($Q = 0.013 \text{ m}^3\text{s}^{-1}$, $Fr = 1.15$ and 1.5) - Bore propagation from left to right.

In the undular bore, a range of particle trajectory patterns were observed with two distinctive trends (Fig. 8). Among the particles released in the upper flow region ($z/d_0 > 0.5$), a significant proportion followed a helicoidal pattern illustrated in Figure 8 (Particles 6a, 6c, 6d, 8b). The particles followed an orbital path beneath the wave crest where they reached a maximum elevation, and were then advected downstream beneath the next wave trough. These orbital trajectories were somehow comparable to the particle motion beneath regular wave crests (Sawaragi 1995), but the entire trajectories were a combination of orbital paths superposed to a downstream advection. When the particles were injected closer to the bed ($z/d_0 < 0.5$), they were often subjected to some recirculation motion, with an initially rapid deceleration followed by an upstream advection behind the bore front. For example in Figure 8 (Bottom), the particles 2, 4c and 5b were recirculated upstream with a advection velocity $V_x/V_0 = -0.5$ in average. The two distinctive trends are illustrated in Figure 8.

In a breaking tidal bore, the particle trajectories were more complicated. Most particles that were injected very close to the bed ($z/d_0 < 0.2$) were subjected to a sudden deceleration and then an upstream motion: e.g., the particle trajectory b8 with red circular symbols in Figure 9. The other particles

were subjected to a pseudo-chaotic motion induced by the large scale turbulent eddies generated in the mixing layer of the bore roller. Some examples of such particle trajectories are presented in Figure 9 (particles b2a, b6a, b9b, b10c).

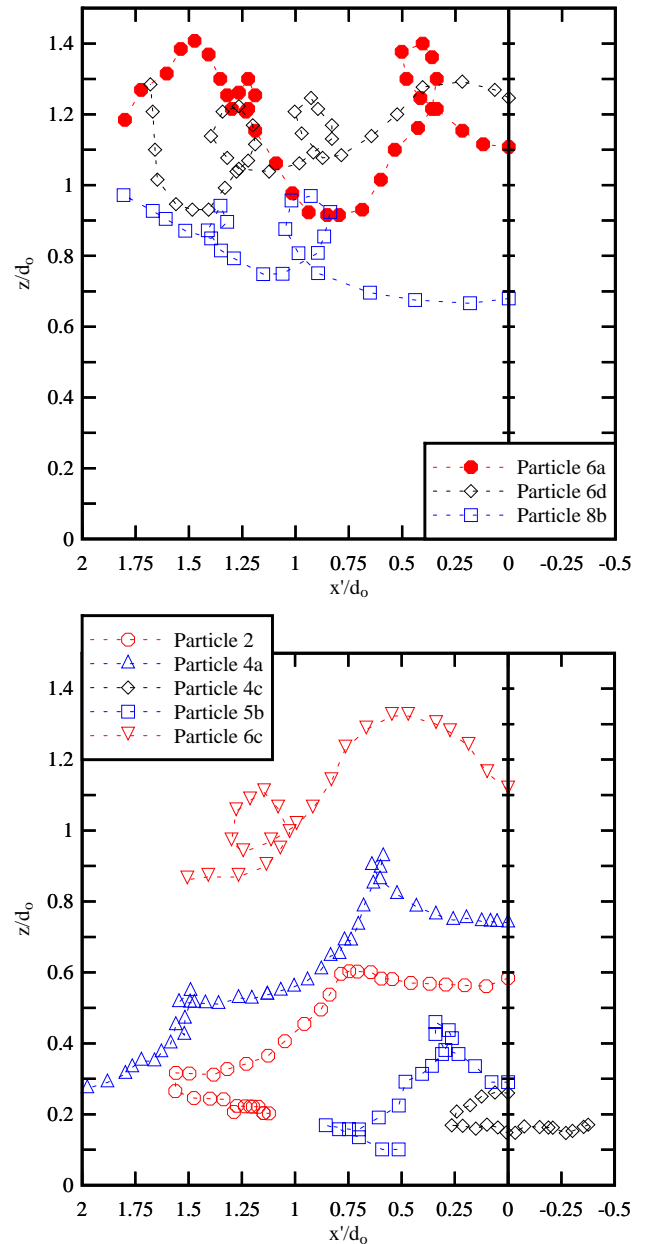


Figure 8: Dimensionless particle trajectories in the undular tidal bore ($Fr = 1.15$, $Q = 0.013 \text{ m}^3\text{s}^{-1}$, $d_0 = 0.0775$ m).

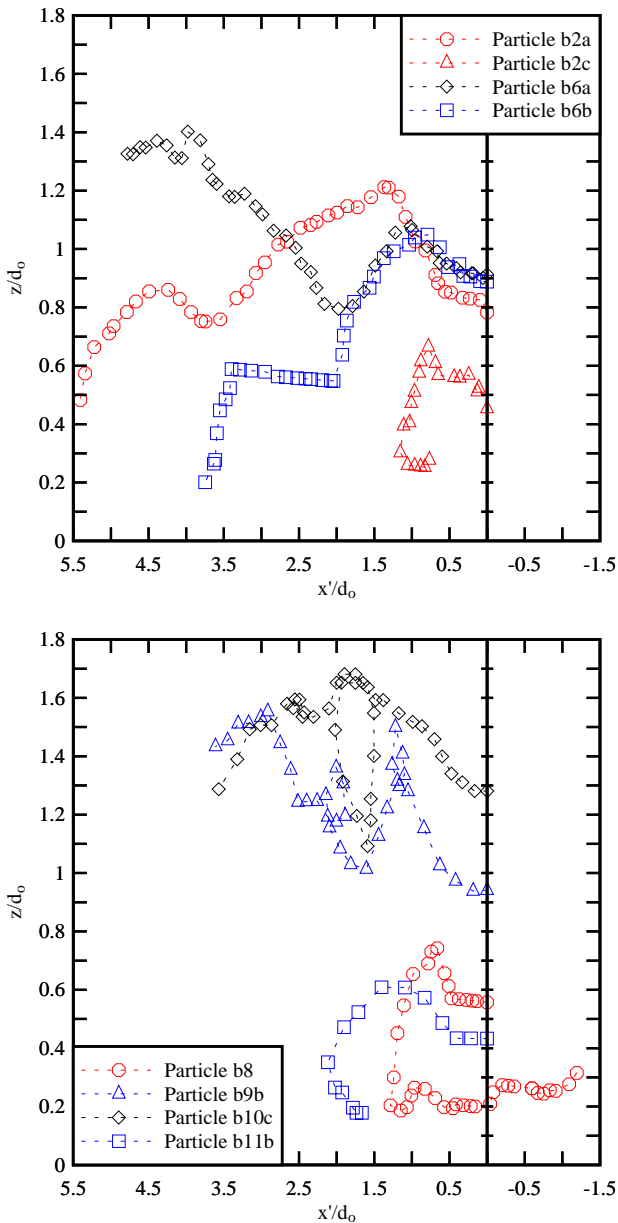


Figure 9: Dimensionless particle trajectories in the breaking tidal bore ($Fr = 1.51$, $Q = 0.013 \text{ m}^3 \text{ s}^{-1}$, $d_o = 0.0505 \text{ m}$).

Particle velocities

Beneath the undular tidal bore, the particle motion data yielded large fluctuations of horizontal and vertical particle velocity components during the undular bore propagation beneath the undulations. The long-lasting impact of the free-surface undulations is a key feature of undular tidal bores in natural systems (Koch and Chanson 2008). The comparative observations with a same initial flow rate suggested that the undular bore induced a greater particle mixing compared to the breaking bore, especially in the upper flow region ($z/d_o > 0.5$).

The ensemble-averaged particle velocity data are presented in Figures 10 and 11 in terms of the dimensionless horizontal and vertical particle velocity components $(V_x)_{avg}/V_o$ and $(V_z)_{avg}/V_o$ respectively. Both figures have identical horizontal and vertical scales. The entire data sets corresponded to a study period of 1.3 s in each case and the time interval between each data point was 1/30 s. The

results presented some common trends as well as highlighted some differences between undular and breaking tidal bores.

In both cases, the light-weight particles were subjected to a rapid deceleration shortly after the bore front passage (Fig. 10 & 11). Next to the bed, some turbulent recirculation motion was observed. The findings were consistent with the turbulence measurements of Koch and Chanson (2009) and Chanson (2010b), and the numerical results of Lubin et al. (2010). The particle recirculatory motion is believed to be caused by the large vortical structures produced next to the bed during the tidal bore propagation.

In the undular bore, however, the particle motion was strongly influenced by the free-surface undulation pattern, including the orbital trajectory motion seen in Figure 8 and large vertical velocity fluctuations (Fig. 10).

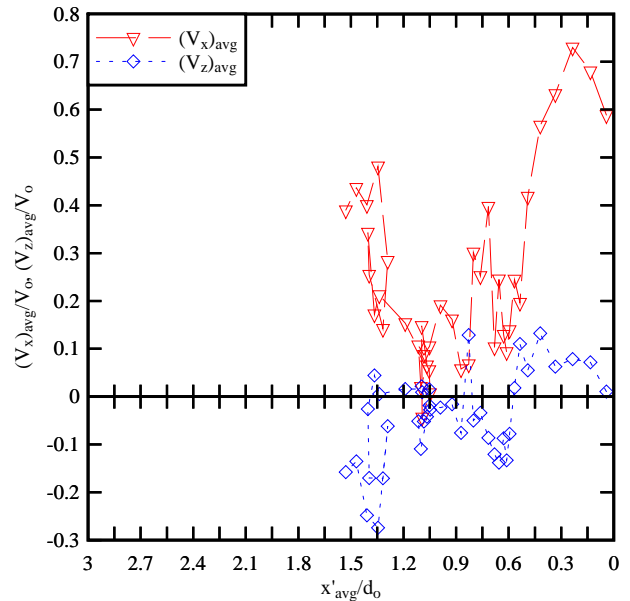


Figure 10: Ensemble-averaged horizontal and vertical particle velocity components beneath an undular tidal bore ($Fr = 1.15$, $Q = 0.013 \text{ m}^3 \text{ s}^{-1}$, $d_o = 0.0775 \text{ m}$).

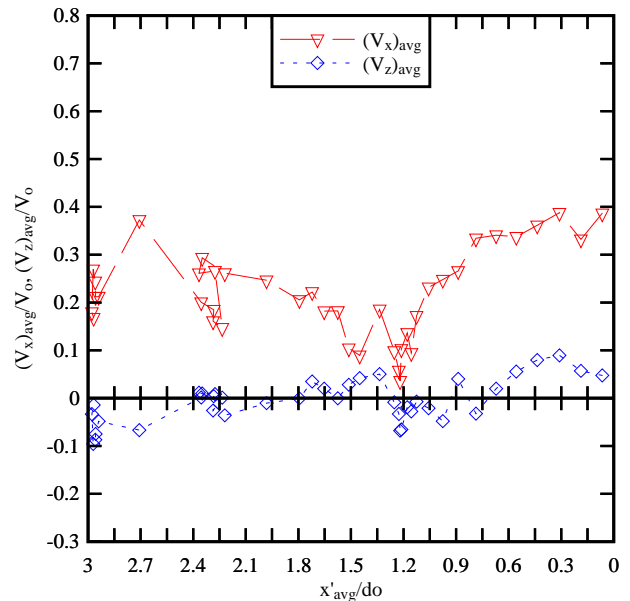


Figure 11: Ensemble-averaged horizontal and vertical

particle velocity components beneath a breaking undular tidal bore ($Fr = 1.51$, $Q = 0.013 \text{ m}^3\text{s}^{-1}$, $d_o = 0.0505 \text{ m}$).

Discussion

Assuming a homogenous, stationary turbulence behind the tidal bore front, the turbulent diffusion coefficient may be estimated from the mean square displacement of the particles:

$$(1) \quad D_x = \frac{\sigma_x^2}{2 t'}$$

$$(2) \quad D_z = \frac{\sigma_z^2}{2 t'}$$

where D_x and D_z are the turbulent mixing coefficients in the x- and z-directions respectively, σ_x and σ_z are respectively the mean square displacement of the particles in the x- and z-directions, and t' is the time scale with $t' = 0$ when the particle passed beneath the leading edge of the bore front. Equations (1) and (2) may be derived using Langevin's model of turbulent dispersion or the random walk model assuming that t' is much larger than the Lagrangian time scale (Pope 2000, Chanson 2004). The experimental results are presented in Figure 11 where q is the discharge per unit width. Herein D_x and D_z characterised the turbulent diffusion of the light-weight particles immediately behind the tidal bore front, and the results are summarised in Table 3. Despite the simplistic assumptions underlying Equations (1) and (2), the data suggested that the longitudinal mixing coefficient was nearly one order of magnitude greater than the vertical diffusion coefficient (Table 3). For comparison, in a fully-developed open channel, the average vertical mixing coefficient is $\epsilon_z/q = 0.067 \sqrt{f/8}$ where f is the Darcy-Weisbach friction factor (Rutherford 1994, Chanson 2004). The present observations of vertical diffusion coefficients behind tidal bores were one order of magnitude larger than the vertical diffusion coefficient in a fully-developed open channel flow, with relatively little difference between undular and breaking tidal bores (Fig. 11). Overall the experimental data highlighted the strong longitudinal and vertical mixing behind both undular and breaking tidal bores.

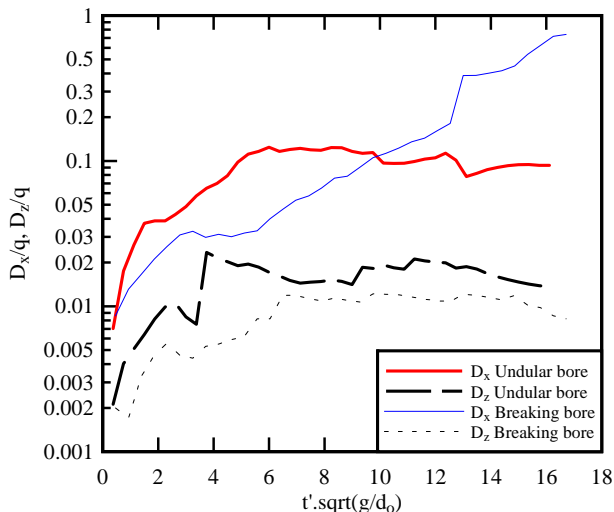


Figure 11: Dimensionless turbulent diffusion coefficients of

particles in the x- and z-directions immediately behind undular and breaking tidal bore fronts.

Tidal bore	V_o ms^{-1}	d_o m	D_x/q	D_z/q	Remark
Undular	0.335	0.0775	0.10	0.018	$8 < t\sqrt{g/d_o} < 14$
Breaking	0.515	0.0505	0.12	0.011	

Table 3: Turbulent diffusion coefficients immediately behind undular and breaking tidal bores (Present study).

A key feature of the present findings is the wide range of particle trajectories and trajectory patterns beneath a tidal bore front, as well as the vortical motion induced by turbulence (Fig. 8 & 9). Both qualitative and quantitative observations implied the existence of large scale vortices in which the light-weight particles were trapped and advected within. Earlier physical and numerical studies documented the production of large coherent structures (Koch and Chanson 2009, Lubin et al. 2010). The energetic turbulent events beneath and shortly after the tidal bore front implied the generation of vorticity in and behind the bore front. The presence of these persisting coherent structures indicated that a great amount of sediment could be placed into suspension and transported by the main flow. The present observations with light-weight particles suggested that the tidal bore process contributes efficiently to the longitudinal dispersion of the eggs, reducing the efficiency of the predators in tidal-bore affected estuaries as proposed by Rulifson and Tull (1999) and Morris et al. (2003).

In a natural system, the fish eggs are typically advected downstream by the ebb tide. The arrival of the tidal bore does induce a marked longitudinal spread of the eggs. Those located in the upper flow region do continue to flow downstream, while the others reverse their course, flowing upstream behind the bore. Simply the tidal bore induces a very rapid longitudinal spread of the eggs with some form of preferential motion depending upon their vertical position in the water column. The lowest, typically heaviest fish eggs are advected upstream immediately after the tidal bore passage. The higher, typically neutrally buoyant eggs located next to the surface continue their journey downstream for sometimes, although the strong flood flow may bring them back into the upper estuary at a later stage of the tide.

Practical considerations

The present findings have a number of limitations. The experimental setup characterised the two-dimensional flow motion. Some qualitative tests were conducted by placing a camera above the channel. The observations indicated that the particles remained qualitatively along the channel centreline, but the visual observations were adversely affected by the free-surface turbulence during and immediately after the bore front propagation. Newer experiments could be conducted using a transparent channel bed, but the technique could only apply to a smooth channel bed.

Furthermore the initial particle relative elevation had some impact on the particle trajectories. For example, the particles released close to the bed tended to remain close to the bottom. It was however extremely difficult to control the initial particle elevation with some accuracy in the turbulent

flow, without impacting adversely the initial flow motion and boundary conditions.

Conclusions

This physical study focused on the turbulent dispersion of light-weight particles beneath a tidal bore. Small particles with properties close to striped bass (*Morone saxatilis*) fish eggs were used and their turbulent dispersion associated with the passage of undular and breaking bores was documented.

The findings were consistent with some earlier experimental and numerical results, including the observations of rapid flow deceleration and flow reversal beneath the breaking bore roller. Some large velocity fluctuations of horizontal and vertical particle velocity components were observed during the undular bore propagation beneath the undulations. Some interesting features were highlighted, including some large-scale motion implying the existence of large coherent vortical structures. These large turbulent eddies must be responsible for some bed erosion and vertical mixing of the water column when a tidal bore propagates upstream in the estuarine zone of a natural system (Fig. 1). The large-scale vortices are also responsible to the longitudinal dispersion of fish eggs reducing the impact of predators. The present results showed that the tidal bore induces a very rapid longitudinal spread of the eggs with some form of preferential motion depending upon their vertical elevation within the water column. The estimates of the longitudinal and vertical diffusion coefficients showed quantitative results that were one to two orders of magnitude larger than those in fully-developed open channel flows, with relatively little difference between undular and breaking tidal bore flow motion.

Finally it must be noted that the present experiments were performed with an unique particle size and density. Future tests should encompass a range of particle sizes and density.

Acknowledgements

The authors acknowledge the technical assistance of Graham Illidge and Clive Booth (The University of Queensland).

References

- Andersen, V.M., Undular Hydraulic Jump." Journal of Hydraulic Division, ASCE, Vol. 104, No. HY8, pp. 1185-1188 (1978)
- Benet, F., and Cunge, J.A., Analysis of Experiments on Secondary Undulations caused by Surge Waves in Trapezoidal Channels. Journal of Hydraulic Research, IAHR, Vol. 9, No. 1, pp. 11-33 (1971)
- British Standard, Flow Measurement. British Standard Code BS 1042:1943, British Standard Institution, London (1943)
- Chanson, H. Environmental Hydraulics of Open Channel Flows. Elsevier-Butterworth-Heinemann, Oxford, UK, 483 pages (2004)
- Chanson, H., Current Knowledge in Tidal bores and their Environmental, Ecological and Cultural Impacts. Environmental Fluid Mechanics, Vol. 10, No. 3 (DOI: 10.1007/s10652-009-9160-5) (2010a)
- Chanson, H., Unsteady Turbulence in Tidal Bores: the Effects of Bed Roughness. Journal of Waterway, Port, Coastal, and Ocean Engineering, ASCE, Vol. 136 (2010b)
- Favre, H., Etude Théorique et Expérimentale des Ondes de Translation dans les Canaux Découverts. Dunod, Paris, France (1935)
- Hornung, H.G., Willert, C., and Turner, S., The Flow Field Downstream of a Hydraulic Jump. Journal of Fluid Mech., Vol. 287, pp. 299-316 (1995)
- Koch, C., and Chanson, H., Turbulent Mixing beneath an Undular Bore Front. Journal of Coastal Research, Vol. 24, No. 4, pp. 999-1007 (DOI: 10.2112/06-0688.1) (2008)
- Koch, C., and Chanson, H., Turbulence Measurements in Positive Surges and Bores. Journal of Hydraulic Research, IAHR, Vol. 47, No. 1, pp. 29-40 (DOI: 10.3826/jhr.2009.2954) (2009)
- Lemoine, R., Sur les Ondes Positives de Translation dans les Canaux et sur le Ressaut Ondulé de Faible Amplitude. Journal La Houille Blanche, Mar-Apr., pp. 183-185 (1948)
- Lubin, P., Glockner, S., and Chanson, H., Numerical Simulation of a Weak Breaking Tidal Bore. Mechanics Research Communications, Vol. 37, No. 1, pp. 119-121 (DOI: 10.1016/j.mechrescom.2009.09.008) (2010)
- Morris, J.A., Rulifson, R.A., and Toburen, L.H., Life History Strategies of Striped Bass, *Morone Saxatilis*, Populations inferred from Otolith Microchemistry. Fisheries Research, Vol. 62, pp. 53-63 (2003)
- Pope, S.B. Turbulent Flows. Cambridge University Press, UK, 771 pages (2000)
- Rulifson, R.A., and Tull, K.A., Striped Bass Spawning in a Tidal Bore River: the Shubenacadie Estuary, Atlantic Canada. Transactions of the American Fisheries Society, Vol. 128, pp. 613-624 (1999)
- Rutherford, J.C. River Mixing. John Wiley, Chichester, USA, 347 pages (1994)
- Sawaragi, T., Coastal Engineering - Waves, Beaches, Wave-Structure Interactions. Elsevier, Developments in Geotechnical Engineering Series, No. 78, Amsterdam, The Netherlands, 479 pages (1995)
- Simpson, J.H., Fisher, N.R., and Wiles, P., Reynolds Stress and TKE Production in an Estuary with a Tidal Bore. Estuarine, Coastal and Shelf Science, Vol. 60, No. 4, pp. 619-627 (2004)

Treske, A., Undular Bores (Favre-Waves) in Open Channels - Experimental Studies. *Journal of Hydraulic Research*, IAHR, Vol. 32, No. 3, pp. 355-370 (1994)

Wolanski, E., Williams, D., Spagnol, S., and Chanson, H., Undular Tidal Bore Dynamics in the Daly Estuary, Northern Australia. *Estuarine, Coastal and Shelf Science*, Vol. 60, No. 4, pp. 629-636 (2004)